

Influences of piles on the ground vibration considering the train-track-soil dynamic interactions

Li, Ting; Su, Qian; Kaewunruen, Sakdirat

DOI:

[10.1016/j.compgeo.2020.103455](https://doi.org/10.1016/j.compgeo.2020.103455)

License:

Creative Commons: Attribution-NonCommercial-NoDerivs (CC BY-NC-ND)

Document Version

Peer reviewed version

Citation for published version (Harvard):

Li, T, Su, Q & Kaewunruen, S 2020, 'Influences of piles on the ground vibration considering the train-track-soil dynamic interactions', *Computers and Geotechnics*, vol. 120, 103455.
<https://doi.org/10.1016/j.compgeo.2020.103455>

[Link to publication on Research at Birmingham portal](#)

General rights

Unless a licence is specified above, all rights (including copyright and moral rights) in this document are retained by the authors and/or the copyright holders. The express permission of the copyright holder must be obtained for any use of this material other than for purposes permitted by law.

- Users may freely distribute the URL that is used to identify this publication.
- Users may download and/or print one copy of the publication from the University of Birmingham research portal for the purpose of private study or non-commercial research.
- User may use extracts from the document in line with the concept of 'fair dealing' under the Copyright, Designs and Patents Act 1988 (?)
- Users may not further distribute the material nor use it for the purposes of commercial gain.

Where a licence is displayed above, please note the terms and conditions of the licence govern your use of this document.

When citing, please reference the published version.

Take down policy

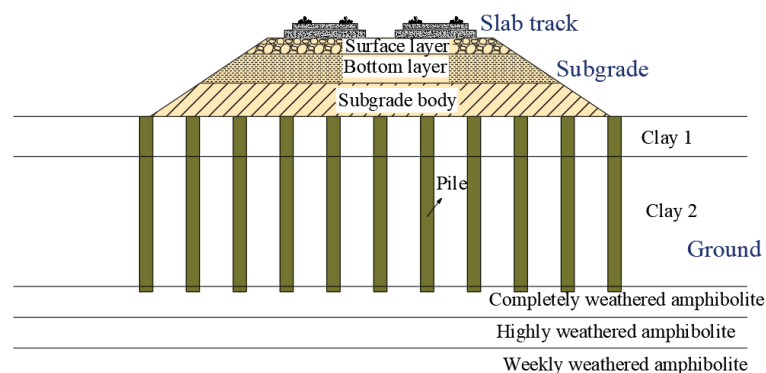
While the University of Birmingham exercises care and attention in making items available there are rare occasions when an item has been uploaded in error or has been deemed to be commercially or otherwise sensitive.

If you believe that this is the case for this document, please contact UBIRA@lists.bham.ac.uk providing details and we will remove access to the work immediately and investigate.

30 **Keywords:** pile effect; ground vibration; critical speed; train-track-soil interactions; perfectly
31 matched layers; wave propagation

32 1. Introduction

33 As one of the most sustainable developments for ground transportation, the high-speed
34 railway has been developed rapidly all over the world over the recent several decades [1-3].
35 The French TGV has reached a record top speed of 574.8 km/h. The Chinese ‘Fuxing’ train is
36 traveling at a speed of 350 km/h in numerous rail networks in China. These high-speed trains
37 can impart higher dynamic forces to rail infrastructures and result in an elevated vibration
38 level for the coupled train-track-soil system [4]. In order to meet the requirements for the
39 high-speed rail system, the slab tracks, highly-compacted subgrade, and pile-reinforced
40 ground are customarily adopted in high-speed railways [5-7], as illustrated in Figure 1.



41

42 **Figure 1 Cross-section of a high-speed railway (adopted from Ref. [7])**

43 The ground-borne vibration induced by the train-track-soil dynamic interactions has
44 received increasing attention recently [8-10]. According to previous studies, high-speed trains
45 traveling on soft soils can significantly increase the vibration level especially when the train
46 moves at the so-called ‘critical speed’, at which the train induces a resonance-like
47 phenomenon [4, 11]. The critical speed depends typically on the Rayleigh wave velocity of
48 soft soils. The measured dynamic displacement of the track can be three times the static value
49 when the train speed is close to the Rayleigh wave velocity at the well-known railway site at
50 Sweden [8, 9]. Many studies have been conducted to investigate the ground vibration of
51 ballasted-track railway under normal and critical train speeds, including the propagation of
52 Rayleigh wave in the soils [12, 13], development of the constitutive model of nonlinear soil

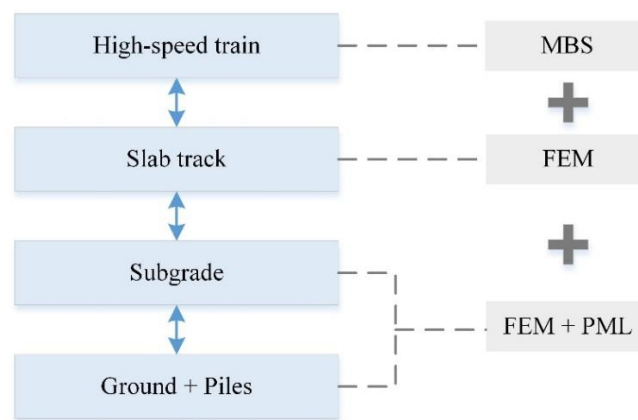
53 with large deformation [14, 15], influence of soil properties on the ground vibration [16, 17],
54 evaluation of the environmental ground vibration [18, 19], and so on. Most previous studies
55 have merely considered the natural ground with soft soils. However, the pile-reinforced
56 ground improvement is widely adopted in soft soil region in high-speed railways since it can
57 significantly reduce both total and differential settlement of soils [20, 21], bringing about an
58 excellent long-term performance during the operation of railways [22, 23]. As the piles can
59 increase the stiffness of soft ground, the vibration responses of railway with pile-reinforced
60 ground will be different from the responses with natural ground. In addition, the previous
61 studies have customarily considered the ground vibration under ballasted track [11, 15-18].
62 However, the use of slab track is getting prevailing in high-speed railways nowadays [5, 6,
63 24]. The slab track can also prompt different railway vibration responses. It is crucial to
64 highlight the influences of piles on the ground vibration in high-speed railway with slab
65 tracks.

66 The high-speed train, slab track, multi-layered subgrade, and pile-reinforced ground are a
67 coupled dynamic interaction system. With the development of computer science, numerical
68 simulation has become an efficient technique to investigate railway vibration responses [3, 25,
69 26]. Although previous researchers such as Thach et al. [27] and Tang et al. [28] developed a
70 numerical model to investigate the vibration responses of railway with pile-reinforced ground,
71 they just simplified the vehicle as the moving load, which is unable to simulate the dynamic
72 excitation effect induced by the train-track interactions with the roughness of rail surface. The
73 2D and 2.5D models have also been developed to analyze the ground vibration responses but
74 these models are still limited in scope due to the plane stress/strain assumptions. In order to
75 overcome these limitations, Kouroussis et al. [16, 17] and Connolly et al. [29, 30] developed a
76 3D coupled train-track-soil numerical model to study the ground vibration responses.
77 However, they just simulated the natural ground without considering any improvements in
78 soft soils.

79 Considering previous studies have merely investigated the natural-ground vibration
80 under ballasted track, a 3D fully coupled train-track-soil model has been developed using
81 LS-DYNA to investigate the piles influences on the ground vibration responses in high-speed
82 railway with slab tracks. The critical speeds of the railway with natural and pile-reinforced

83 grounds have been highlighted firstly. The vibration responses of the railway have then been
84 evaluated. Besides, it is original to discuss the influences of piles on the wave propagations in
85 the soils with natural and pile-reinforced grounds. This study could bring an insightful and
86 better understanding of the vibration responses of high-speed railway with pile-reinforced
87 ground and slab track for the design, operation, and maintenance for the rail system in
88 practice.

89 2. Modeling of the train-track-soil dynamic interactions



90

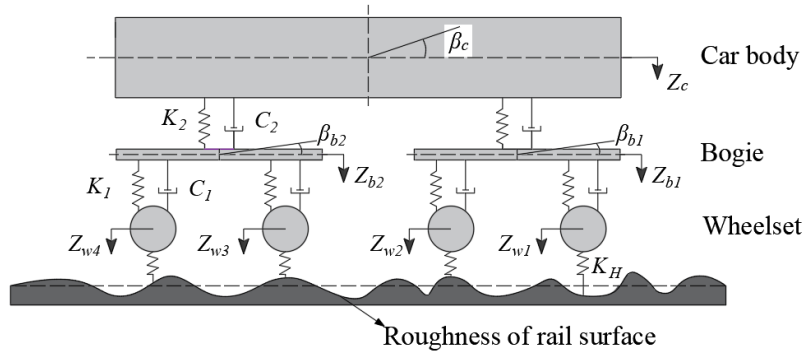
91 Figure 2 Coupling of the train-track-soil system

92 A novel 3D coupled train-track-soil model is developed using LS-DYNA to investigate
93 the influences of piles on the ground vibration in high-speed railway with slab tracks. The
94 high-speed train is simulated based on the multi-body simulation (MBS) principle, and the
95 slab track is developed based on the finite element modeling (FEM) theory. Besides, the
96 subgrade and pile-reinforced ground are simulated based on the FEM theory together with the
97 Perfectly Matched Layers (PML) method, as illustrated in Figure 2.

98 2.1 Modeling of the high-speed train and slab track

99 The coupled train-track-soil dynamic system is developed based on a typical
100 cross-section in Beijing-Shanghai high-speed railway in China [7]. The vehicle commonly
101 operated on this section is the China Railway High-speed (CRH) 380 Electric Multiple Unit
102 (EMU) train. In this simulation model, the vehicle consists of one car body, two bogies, four
103 wheelsets, and two stage-suspension systems, as shown in Figure 3. The car body, bogies, and

104 wheelsets are simplified as the rigid-bodies with shell and beam elements. These
 105 multi-rigid-bodies are connected by the springs and dashpots. As the vertical vibration is the
 106 primary excitation to the infrastructures, the vertical degrees of freedom (DOF) of the vehicle
 107 are considered in this model. The vehicle has totally 10 DOF including the vertical and pitch
 108 motion of car body (Z_c, β_c), the vertical and pitch motion of bogies ($Z_{bi}, \beta_{bi} \ i = 1, 2$), and
 109 the vertical motion of wheelsets ($Z_{wi} \ i = 1, \dots, 4$).



110

111

Figure 3 Simulation of the vehicle

112 The China Railway Track System (CRTS) II slab track is adopted in this railway. It
 113 consists of rail, rail pads, concrete slab, cement asphalt (CA) mortar layer, and concrete base
 114 [31]. The rail is simulated as the Euler beam, which is supported by the discrete springs and
 115 dashpots to represent the rail pads. The concrete slab, CA mortar, and concrete base are
 116 simulated as solid elements.

117 The contact between wheel and rail is simulated based on the Hertz contact theory. The
 118 wheel-rail contact force can be calculated automatically by LS-DYNA based on the following
 119 equation:

120

$$F = K_H \times (Z_w - Z_r - \delta) \quad (1)$$

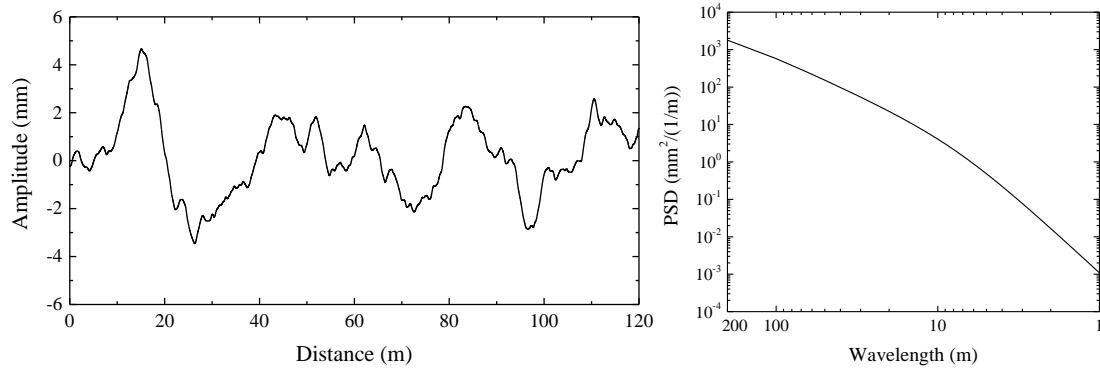
121 Where K_H is the vertical stiffness of the wheel-rail contact spring, $K_H = 1.325 \times 10^9$ N/m in
 122 this study [32]; Z_w is the vertical displacement of the wheel; Z_r is the vertical displacement of
 123 the rail; and δ is the roughness of rail surface.

124 The Germany high-speed low disturbance irregularity is used to excite the wheel-rail
 125 contact. The power spectrum density (PSD) function of the roughness is calculated as follows:

126

$$S_v(\Omega) = \frac{A_v \Omega_c^2}{(\Omega^2 + \Omega_r^2)(\Omega^2 + \Omega_c^2)} \quad (2)$$

127 Where A_v is the roughness constant ($A_v = 4.032 \times 10^{-7} \text{ m}^2 \cdot \text{Rad/m}$); Ω_c and Ω_r are the cutoff
 128 frequency ($\Omega_c = 0.8246 \text{ rad/m}$, $\Omega_r = 0.0206 \text{ rad/m}$); and Ω is the spatial frequency of the
 129 roughness. The PSD function can be transformed into vertical roughness along the
 130 longitudinal distance of the track using a time-frequency transformation technique, as shown
 131 in Figure 4.



132 (a) Roughness with distance

133 (b) PSD with wavelength

134 Figure 4 The roughness of rail surface

135 The material properties of the CRH380 EMU Train and CRTS II slab track are shown in
 136 Table 1. Since most previous studies adopted static material properties of slab track despite
 137 the fact that the actual loads from high-speed trains onto slab tracks are dynamic excitation,
 138 the dynamic material properties of CRTS II slab track are used in this model in order to obtain
 139 a more realistic vibration response. The stiffness of rail pads is determined by the dynamic
 140 value, and the moduli of elasticity of concrete slab, CA mortar, and concrete base are
 141 considered as the strain-rate dependent values [33, 34].

142 Table 1 Properties of the vehicle and slab track

| Properties | Values |
|---|--------------------|
| CRH380 EMU Train | |
| Mass of the car body (kg) | 40,000 |
| Mass of the bogie (kg) | 3,200 |
| Mass of the wheelset (kg) | 2,400 |
| Inertia of pitch motion of the car body(kg.m ²) | 5.47×10^5 |
| Inertia of pitch motion of the bogie(kg.m ²) | 6,800 |
| Primary suspension stiffness (N/m) | 1.04×10^6 |
| Primary suspension damping (N.s/m) | 5×10^3 |
| Secondary suspension stiffness (N/m) | 4×10^5 |
| Secondary suspension damping (N.s/m) | 6×10^3 |
| CRTS II slab track | |
| Mass density of the rail (kg/m ³) | 7,830 |

| | |
|--|---|
| Modulus of elasticity of the rail (Pa) | 2.059×10 ¹¹ |
| Poisson's ratio of the rail | 0.3 |
| Stiffness of the rail pads (N/m) | 5.0×10 ⁷ (dynamic stiffness) |
| Damping of the rail pads (N.s/m) | 7.5×10 ⁴ |
| Mass density of the concrete slab (kg/m ³) | 2,500 |
| Modulus of elasticity of the concrete slab (Pa) | 3.6×10 ¹⁰ (reference static value, strain-rate dependent) |
| Poisson's ratio of the concrete slab | 0.2 |
| Mass density of the CA mortar (kg/m ³) | 1,900 |
| Modulus of elasticity of the CA mortar (Pa) | 7×10 ⁹ (reference static value, strain-rate dependent) |
| Poisson's ratio of the CA mortar | 0.2 |
| Mass density of the concrete base (kg/m ³) | 2,400 |
| Modulus of elasticity of the concrete base (Pa) | 2.55×10 ¹⁰ (reference static value, strain-rate dependent) |
| Poisson's ratio of the concrete base | 0.2 |

143 2.2 Modeling of the soil

144 The subgrade consists of three layers in the Beijing-Shanghai high-speed railway:
145 surface layer, bottom layer, and subgrade body. The ground consists of five layers: clay 1,
146 clay 2, completely weathered amphibolite, highly weathered amphibolite, and weekly
147 weathered amphibolite, as illustrated in Figure 1. The soils are simulated as viscoelastic
148 material using solid elements. In addition, since the amphibolite is a type of rock, and the
149 stiffness of amphibolite is much higher than that of clay [7], the three layers of the
150 amphibolite are not developed in the model, and the fixed boundary is set at the bottom of the
151 second layer of ground instead.

152 To prevent spurious wave reflections from the truncated boundary, perfectly matched
153 layers (PML) method, which is the most efficient infinite boundary, is used in this simulation
154 model. PML is set parallel to the FEM domain, and it can perfectly attenuate the outgoing
155 waves and then reflect them with arbitrarily small amplitudes back to the FEM domain [35,
156 36], as illustrated in Figure 5.

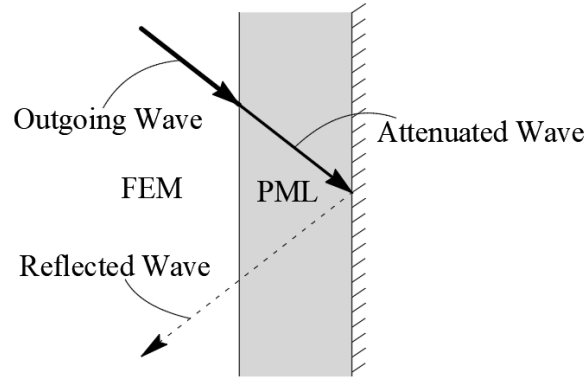


Figure 5 Absorbing boundary of PML

The material properties of soils are measured from the section of the Beijing-Shanghai high-speed railway, as shown in Table 2. Note that most in-site tests cannot give precise information on the damping of internal soils. In order to minimize the gap between the experimental and numerical dynamic responses of the soil, the Rayleigh damping of soil is usually used in the simulation models [29, 30]. The damping matrix is defined as:

$$[\mathbf{C}] = \alpha[\mathbf{M}] + \beta[\mathbf{K}] \quad (3)$$

Where \mathbf{M} and \mathbf{K} are the mass and stiffness matrix of the whole FEM model, respectively; and α and β are the coefficients. In this model, $\alpha = 0$ and $\beta = 0.0002$ [17].

Table 2 Properties of soils and pile (c_p : P wave velocity; c_s : S wave velocity; c_R : Rayleigh wave velocity)

| Components | Depth (m) | Density (kg/m ³) | Modulus of elasticity (MPa) | Poisson's ratio | c_p (km/h) | c_s (km/h) | c_R (km/h) |
|---------------------------|-----------|------------------------------|-----------------------------|-----------------|--------------|--------------|--------------|
| Surface layer of subgrade | 0.4 | 2300 | 200 | 0.25 | 1162.90 | 671.40 | 616.08 |
| Bottom layer of subgrade | 2.3 | 1950 | 150 | 0.35 | 1264.91 | 607.64 | 567.58 |
| Subgrade body | 2 | 2100 | 110 | 0.3 | 955.95 | 510.98 | 473.24 |
| First layer of ground | 2.4 | 1900 | 42 | 0.3 | 621.01 | 331.94 | 307.43 |
| Second layer of ground | 13.1 | 2010 | 83 | 0.36 | 948.39 | 443.57 | 415.00 |
| Pile | 15.5 | 2200 | 7000 | 0.2 | - | - | - |

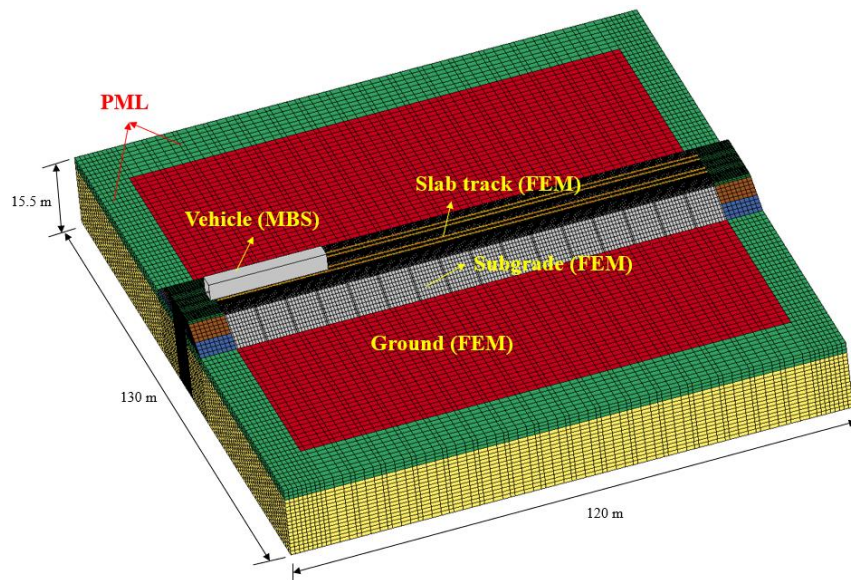
2.3 Modeling of the pile

The cement fly-ash gravel (CFG) piles are adopted in the soft soils in Beijing-Shanghai high-speed railway to improve the serviceability of the ground [7]. The length of the piles is 15.5 m. The diameter and spacing of the piles are 0.5 m and 1.8 m, respectively.

173 In the simulation model, the beam element is used to simulate piles to improve the
174 computational efficiency, and the shared node method is adopted for the piles and soils.
175 Unlike the cyclic dynamic loads, the monotonic train loads cannot induce the consolidation of
176 soft soils, and the differential deformation between piles and soils is relatively small, so the
177 friction between piles and soils is neglected in this model [37, 38]. The material properties of
178 the piles are shown in Table 2.

179 2.4 Computational implementation

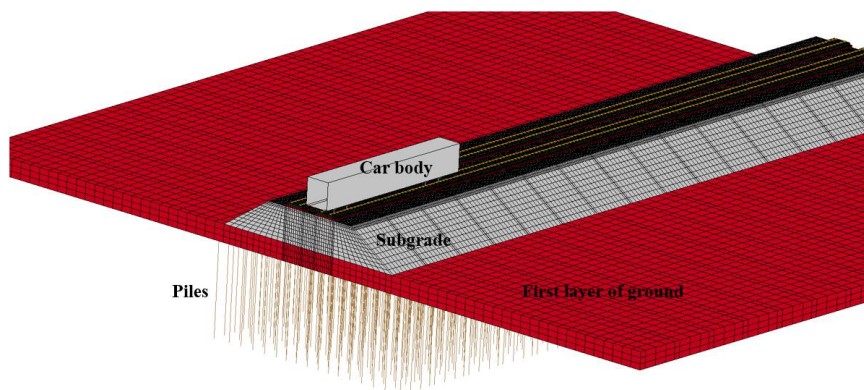
180 The dimension of the whole model is 120 m × 130 m × 15.5 m, as illustrated in Figure 6.
181 It is noted that the Beijing-Shanghai high-speed railway line is a double-track railway,
182 indicating that the model cannot be developed as a half model from the center of the railway
183 since the dynamic train load is not always symmetrical.



184

185

(a) Whole model



186

187 (b) Pile-reinforced ground model

188 Figure 6 Numerical model in LS-DYNA

189 The wheel-rail contact is developed using the built-in keywords in LS-DYNA:
190 *RAIL_TRACK and *RAIL_TRAIN. In these keywords, a realistic roughness of rail surface
191 and a contact stiffness can be defined by users.

192 Eight layers of solid elements are created around the soil for the PML elements, which
193 are defined by the material: *MAT_PML_ELASTIC. The PML elements have identical
194 properties to the FEM elements.

195 As the dynamic material properties of the slab track are considered, the keyword
196 *MAT_STRAIN_RATE_DEPENDENT_PLASTICITY is used to describe the strain-rate
197 dependent modulus of elasticity.

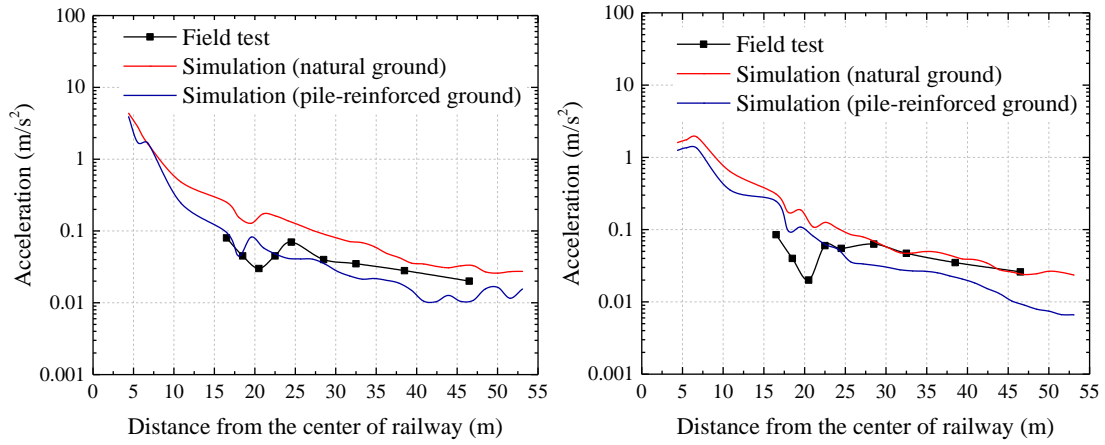
198 The model is developed as two types: model with natural ground and model with
199 pile-reinforced ground, to investigate the influences of piles on the ground vibration. The
200 natural ground model has 399,386 elements, and the pile-reinforced ground model has
201 419,798 elements, including beam elements, shell elements, solid elements, springs, and
202 dashpots.

203 The vehicle is set to travel at a constant speed over the rail after the dynamic relaxation.
204 The explicit central difference method is used to integrate the equations of motion of the
205 coupled train-track-soil system by LS-DYNA with a time step of 1.23×10^{-5} s.

206 **3. Model validation**

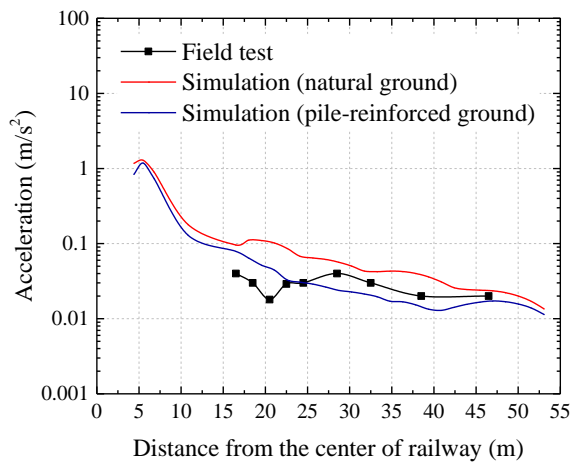
207 **3.1 Acceleration of ground**

208 The acceleration of the environmental ground has been measured in the
209 Beijing-Shanghai high-speed railway with a train speed of 300 km/h [7]. This model can thus
210 be validated by comparing the acceleration from the numerical model against the field-test
211 results, as illustrated in Figure 7.



(a) Vertical acceleration

(b) Lateral acceleration



(c) Longitudinal acceleration

Figure 7 Validation results of ground vibration

The accelerations of soils from the numerical simulations are in good agreement with the field-test results. Although there are differences between these results due to some assumptions of numerical models, the differences are considerably small. The amplitudes in vertical, lateral, and longitudinal directions are less than 0.3 m/s^2 when the distance is longer than 16.5 m. The acceleration in natural ground is higher than that in pile-reinforced ground, indicating the piles can attenuate the ground vibration responses. Therefore, the numerical model developed in this study can predict the ground vibration responses for railways in practice.

3.2 Train-track interactions

The wheel-rail contact responses have not been obtained from the Beijing-Shanghai

227 high-speed railway. In order to validate the train-track interactions, the calculated wheel-rail
 228 contact responses are compared with the field-test results from the Suining-Chongqing
 229 railway, which is constructed to investigate the dynamic performance of vehicle and slab
 230 tracks. The material properties of vehicle and slab track are adopted according to this railway
 231 [39].

232 Table 3 Validation results of train-track dynamic interactions

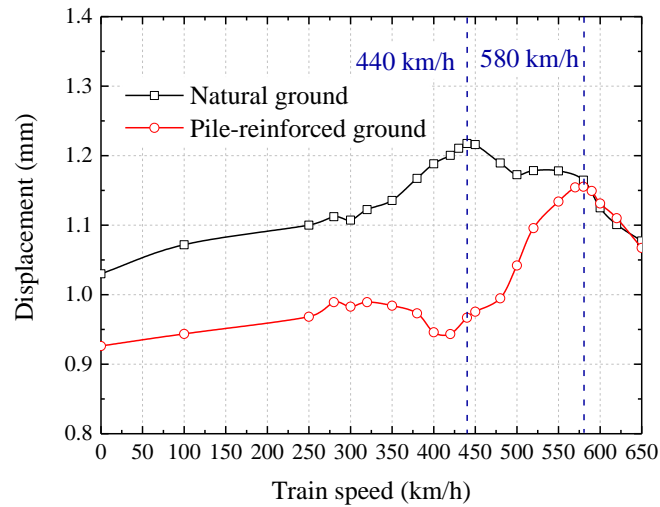
| | Field-test results [39] | Simulation results from Cai et al. [40] | Simulation results from this study |
|-------------------------------|----------------------------|--|---------------------------------------|
| Wheel-rail contact force (kN) | 81-116 | 98.7 | 96.3 |
| Rail pad force (kN) | 14.4-65.8 | 37.648 | 35.1 |
| Displacement of the rail (mm) | 0.3-0.88 | 0.827 | 0.863 |

233 The train-track interactions obtained from the field test, simulation model from Cai et al.,
 234 and simulation model from this study are compared in Table 3. The simulation results from
 235 this model are considered to be within an acceptable range relative to the field-test results,
 236 and also match with the simulation results from Ref.[40]. In sum, the train-track interactions
 237 established in this study also exhibit a good agreement with the field-test results and other
 238 simulation results.

239 4. Results

240 In order to investigate the effects of piles on the ground vibration, the critical speed of
 241 the Beijing-Shanghai high-speed slab-track railway is calculated from the natural and
 242 pile-reinforced ground models firstly. The vibration responses of soils are then analyzed under
 243 normal and critical speeds. The train-track dynamic interactions are also investigated for
 244 comparisons under natural and pile-reinforced ground cases.

245 **4.1 Critical speed**



246

247

Figure 8 Maximum displacement of rail with train speed

248

The maximum dynamic displacements of rail in natural and pile-reinforced ground cases are shown in Figure 8 when the train speed is increased from 0 km/h to 650 km/h. Although a speed of 650 km/h is much higher than the normal operational train speed (≤ 400 km/h), this study is aimed at demonstrating the critical speeds of the high-speed slab-track railway with natural and pile-reinforced ground.

253

In Figure 8, the displacements from the natural ground case are much higher than those from the pile-reinforced ground case. Therefore, the pile exhibits a significant attenuation effect on the ground vibration responses before the train achieves a speed of 580 km/h.

256

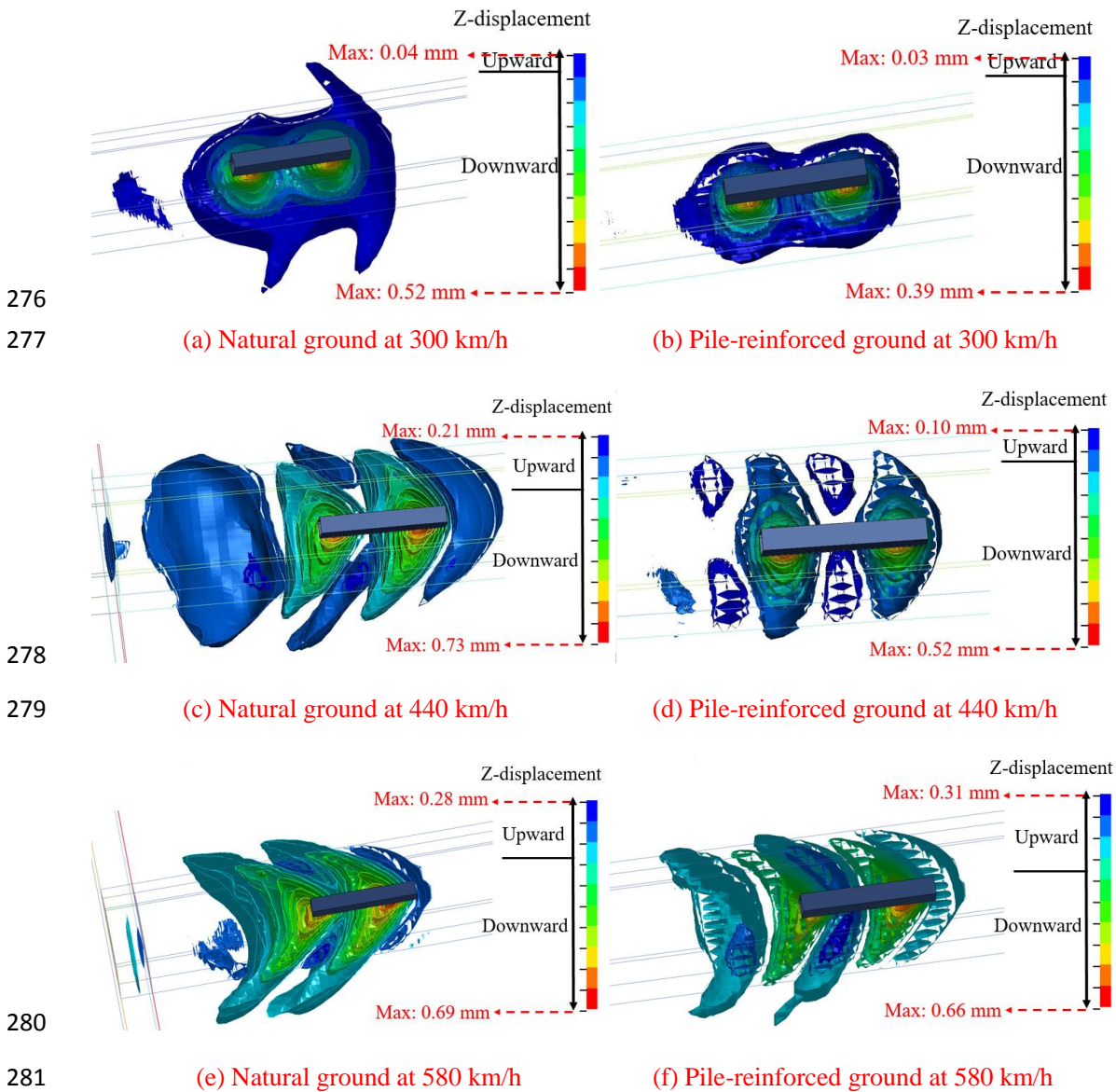
When the piles are not considered, the critical speed of the slab-track railway is around 440 km/h. Unlike the amplification effect in the ballasted track [8, 9], the increased displacement in slab track at critical speed is insignificant, which is rather similar to a previous study in Ref. [41]. The displacement is increased by 18.4% from 1.03 mm (at 0 km/h) to 1.22 mm (at 440 km/h). It is likely that slab track exhibits a higher global track stiffness than conventional ballasted track, leading to a smaller amplification of resonance-like phenomenon. In addition, the critical speed in this model, 440 km/h, is not close to Rayleigh wave velocities of any soil layers. In previous studies, the subgrade is normally simplified as the isotropic material, so the critical speed is normally determined by the Rayleigh wave velocity of the subgrade or the first layer of ground [8, 9, 41]. However, there are five layers

265

266 of soils in this study. The trapezoidal three layers of subgrade and five types of soil properties
267 make the propagation of both surface and body waves complicated.

268 When the piles are considered, the critical speed is increased to 580 km/h. The
269 displacement is increased by 25% from 0.926 mm (at 0 km/h) to 1.16 mm (at 580 km/h). This
270 amplification effect is more significant than that of natural ground case. Also, this critical
271 speed is still generated by five layers of soils but with higher stiffness.

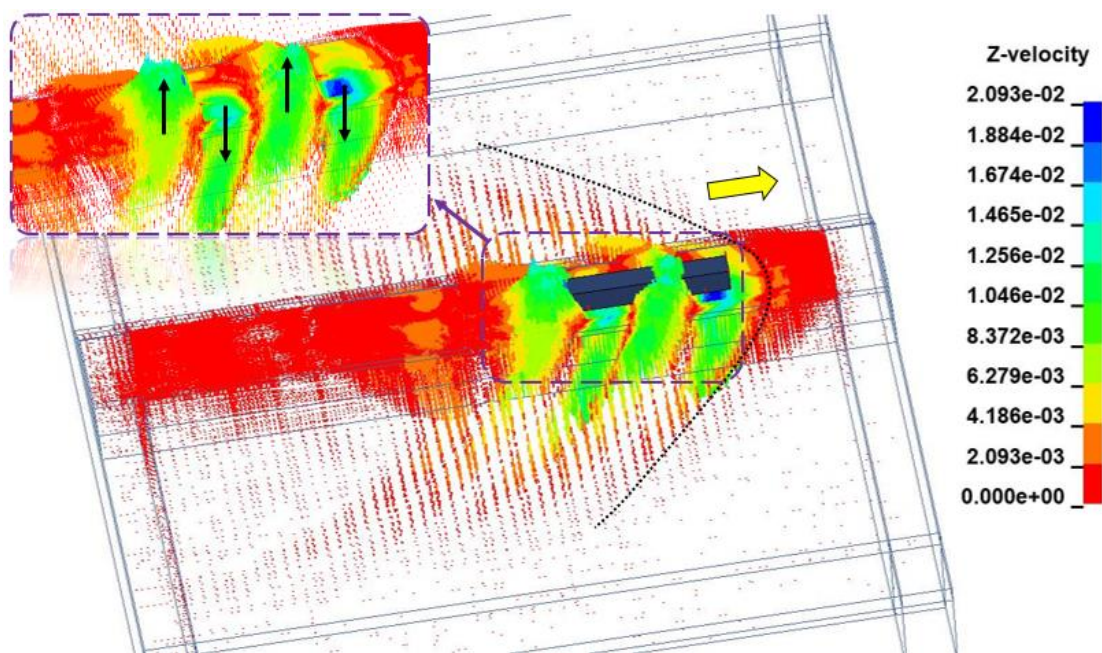
272 It is also noticeable that the critical speed of slab-track railway is much higher than the
273 current operational train speed whether the piles are considered or not. Besides, the
274 amplification effect at critical speed is insignificant, indicating the slab track possesses an
275 excellent dynamic performance.



282 Figure 9 Contours of displacement of the soils

283 The contours of displacement of soils under three train speeds (normal speed and two
284 critical speeds) are illustrated in Figure 9. When the train speed is 300 km/h, the contours of
285 the dynamic displacements are concentrated in a small range of soils. The piles can
286 significantly reduce the downward displacement but have no obvious influence on the upward
287 displacement. When the train travels at 440 km/h, the Mach cone phenomenon, which is
288 analogous to a boat moving through the water, can be observed in the natural ground case.
289 This phenomenon cannot be observed in pile-reinforced ground case at 440 km/h. In addition,
290 since this speed is the critical speed for natural ground case, both upward and downward
291 displacements of soils are higher than those of pile-reinforced ground case. When the train
292 speed reaches to 580 km/h, the piles have no obvious influence on the amplitudes of the
293 displacements, but the Mach cone phenomenon can be observed in both natural and
294 pile-reinforced ground cases.

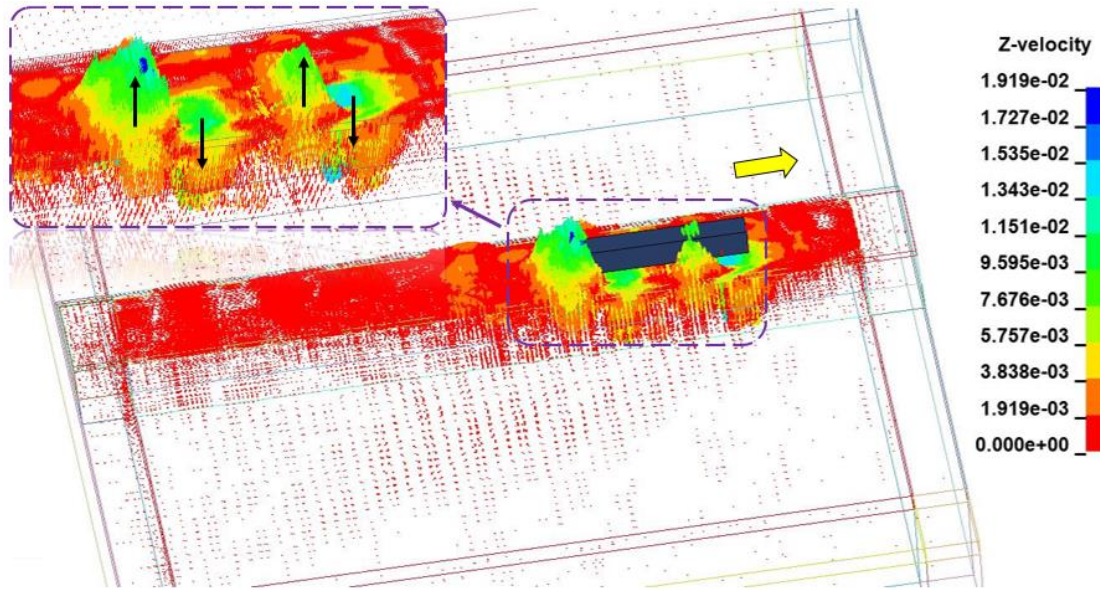
295 **4.2 Dynamic responses of soils**



296

297

(a) Natural ground



(b) Pile-reinforced ground

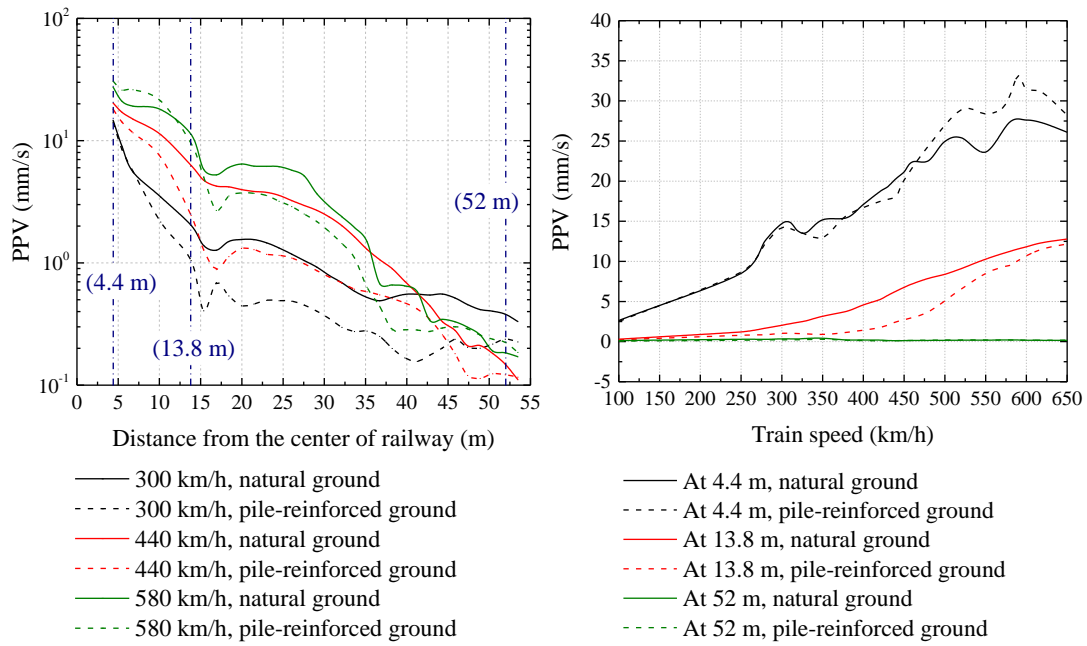
Figure 10 Vectors of the vertical velocity of soils

The vectors of the vertical velocity of soils with natural and pile-reinforced ground are illustrated in Figure 10. The vehicle is running from left side to right side with a speed of 440 km/h. When the piles are disregarded, the influence range of the velocity is quite extensive in the soils, and the Mach cone phenomenon is distinct as illustrated in Figure 10 (a). When the piles are considered, the velocity mainly affects the range of the subgrade, as shown in Figure 10 (b). The velocity of soils exhibits alternating directions: downward-upward-downward-upward, which corresponds with the position of wheelsets. Besides, it is noted that the maximum velocities of the natural and pile-reinforced ground cases are 20.93 mm/s and 19.19 mm/s, respectively, indicating the pile has a small influence on the maximum velocity of soils.

The peak particle velocity (PPV) is usually used to evaluate the dynamic influences on the surrounding environment [16, 17]. It is calculated as follows:

$$PPV = \max|v(t)| \quad (4)$$

Where $v(t)$ is the time-history of the velocity of the soil.



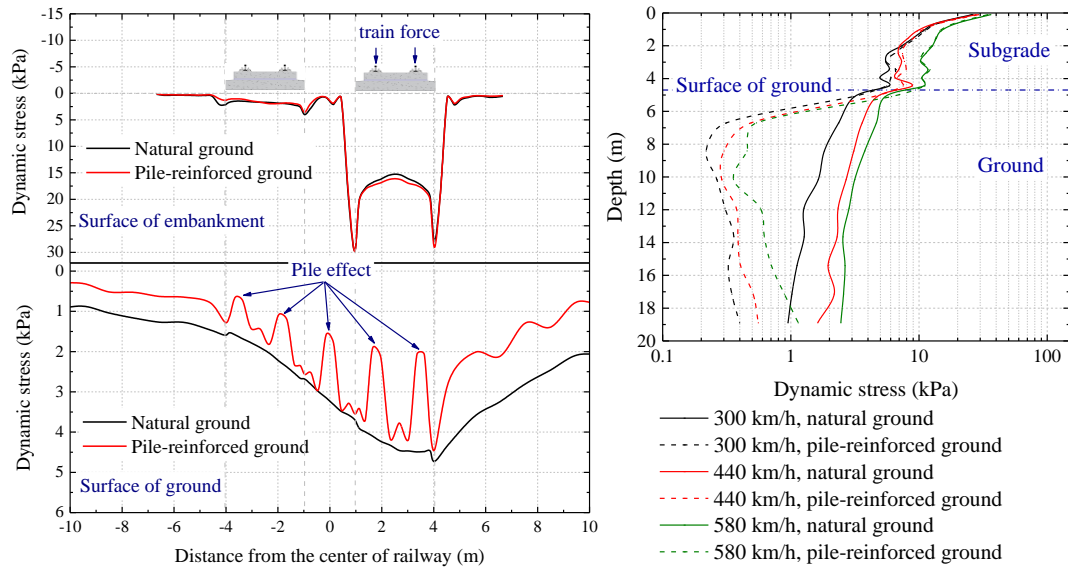
(a) PPV with distance

(b) PPV with train speed

Figure 11 PPV with distance and train speed

The PPV with various distances from the center of railway under three train speeds are shown in Figure 11 (a). The PPV decreases along the overall distance. However, two amplifications which are induced by the reflections of the body waves, occur at around 20 m and 45 m. The piles can significantly reduce the PPV of soils, but the reduction effect is decreased when the train speed is increased.

The PPV with various train speeds are shown in Figure 11 (b). The PPV increases with train speed at 4.4m. The piles have no evident influence on the PPV when the train speed is lower than 300 km/h, but they slightly increase the PPV when the train speed is higher than 460 km/h. Note that the location at 4.4 m is relatively close to the center of railway, so the PPV is significantly influenced by the roughness of rail surface. The piles can considerably reduce the PPV at 13.8 m, which is located at the edge of the pile's foundation. Also, the PPV starts to increase substantially from 300 km/h in the natural ground case, but it starts to increase from 400 km/h in the pile-reinforced ground case. At 52 m, which is far away from the train-track dynamic excitation, the PPV has a small amplitude, and the piles have a minor influence on the ground vibration responses.



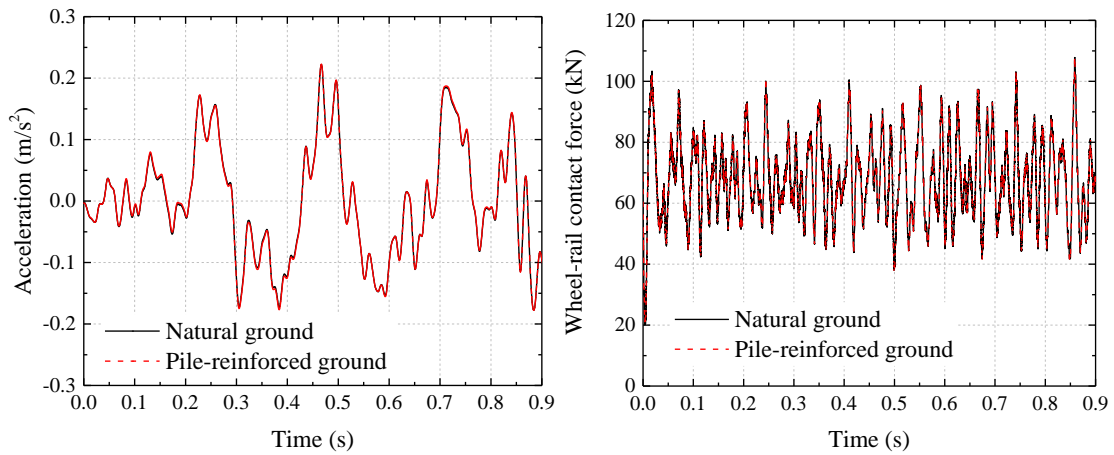
(a) Lateral distribution

(b) Vertical distribution

Figure 12 Dynamic stresses of soils

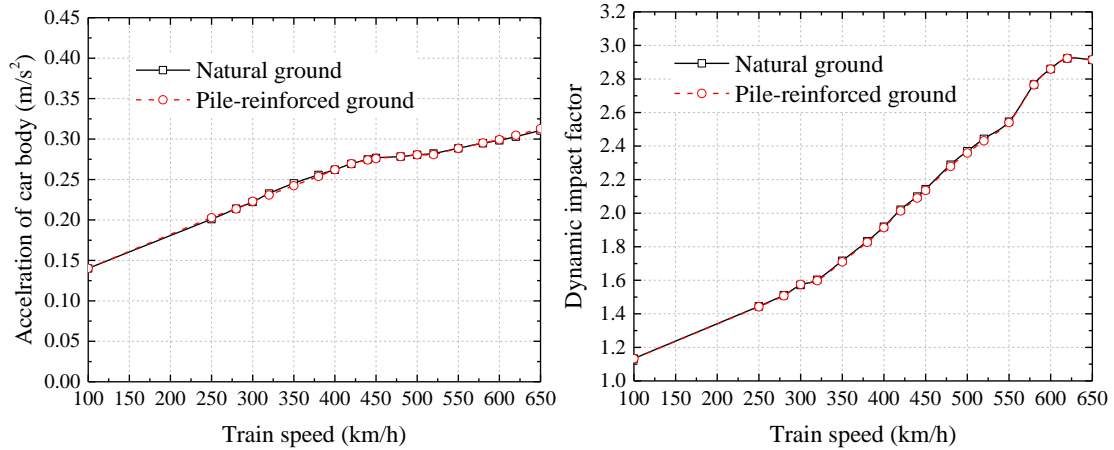
The lateral distributions of the dynamic stresses at the surface of the embankment and ground are illustrated in Figure 12 (a) when the train travels at 440 km/h. The piles have no evident influence on the dynamic stresses of the embankment. The maximum dynamic stress occurs at the edge of the slab track, and a similar phenomenon can be found from Ref.[41]. However, piles can significantly reduce the dynamic stress of the ground especially when the positions are above the piles.

The attenuation effect of dynamic stress along with the depth is shown in Figure 12 (b). The dynamic stresses in the subgrade are in the range of 5 kPa to 37 kPa under three train speeds, but the piles have an insignificant influence on the stresses. In the ground, the dynamic stresses are lower than 9 kPa, and the piles can dramatically reduce the amplitudes.



347
348 (a) Time history of acceleration of car body

(b) Time history of wheel-rail contact force



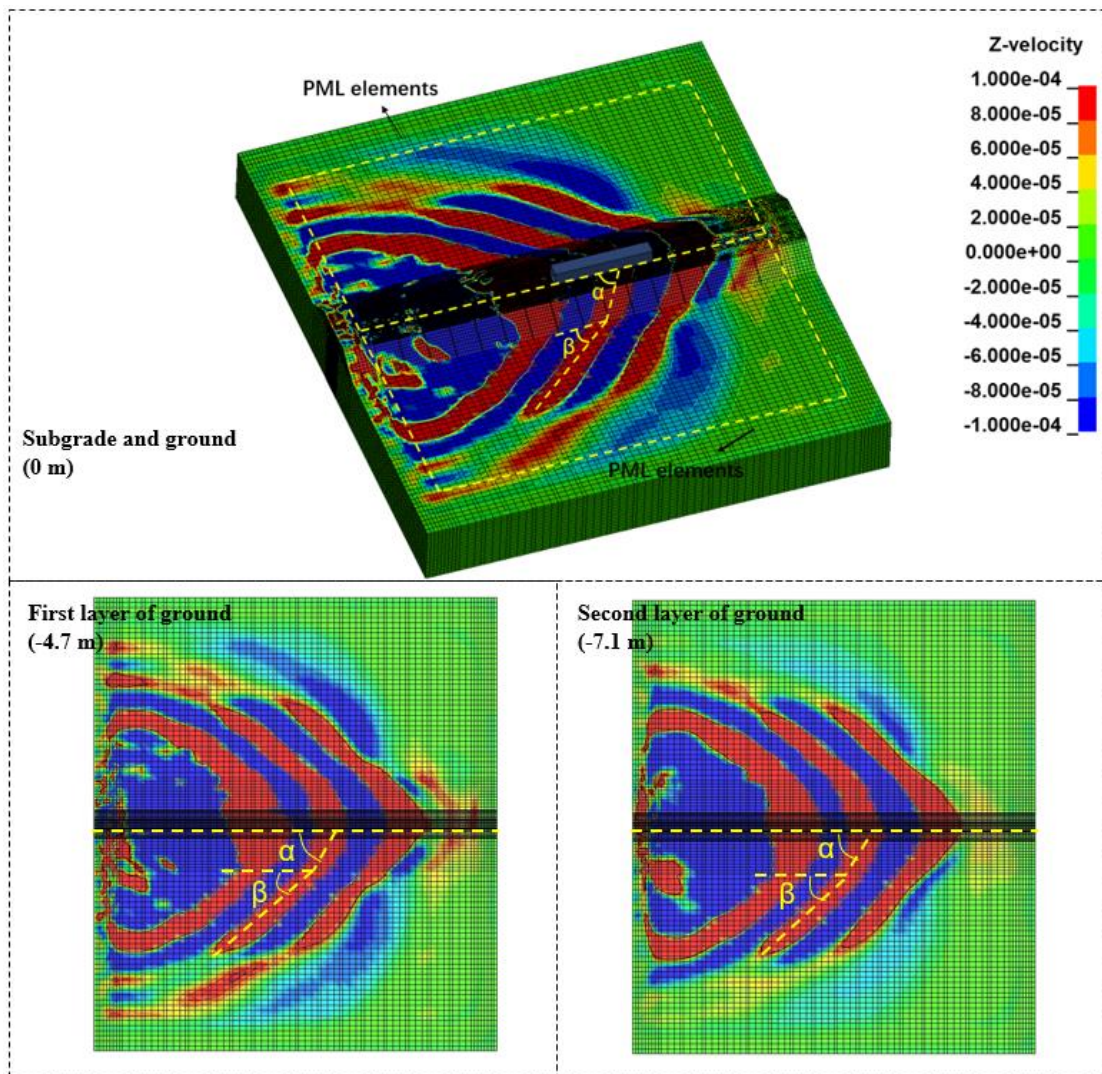
349
350 (c) Acceleration of car body with train speed (d) Dynamic impact factors with train speed

351 **Figure 13 The train-track interaction responses**

352 Figure 13 illustrates the acceleration of the car body and the wheel-rail contact force
 353 under natural and pile-reinforced ground cases. The time history curves of acceleration of car
 354 body and wheel-rail contact force exhibit no evident difference in natural and pile-reinforced
 355 ground cases when the train speed is 300 km/h. The amplitudes of acceleration of car body
 356 and dynamic impact factors significantly increase when the train speed is increased. However,
 357 there is still no obvious difference between the results from natural and pile-reinforced ground
 358 cases, indicating the piles do not influence the train-track interactions. It is likely that the
 359 different displacement between the wheel and rail is considered too small to induce
 360 significant influences on the train-track interaction responses.

361 **5. Discussion**

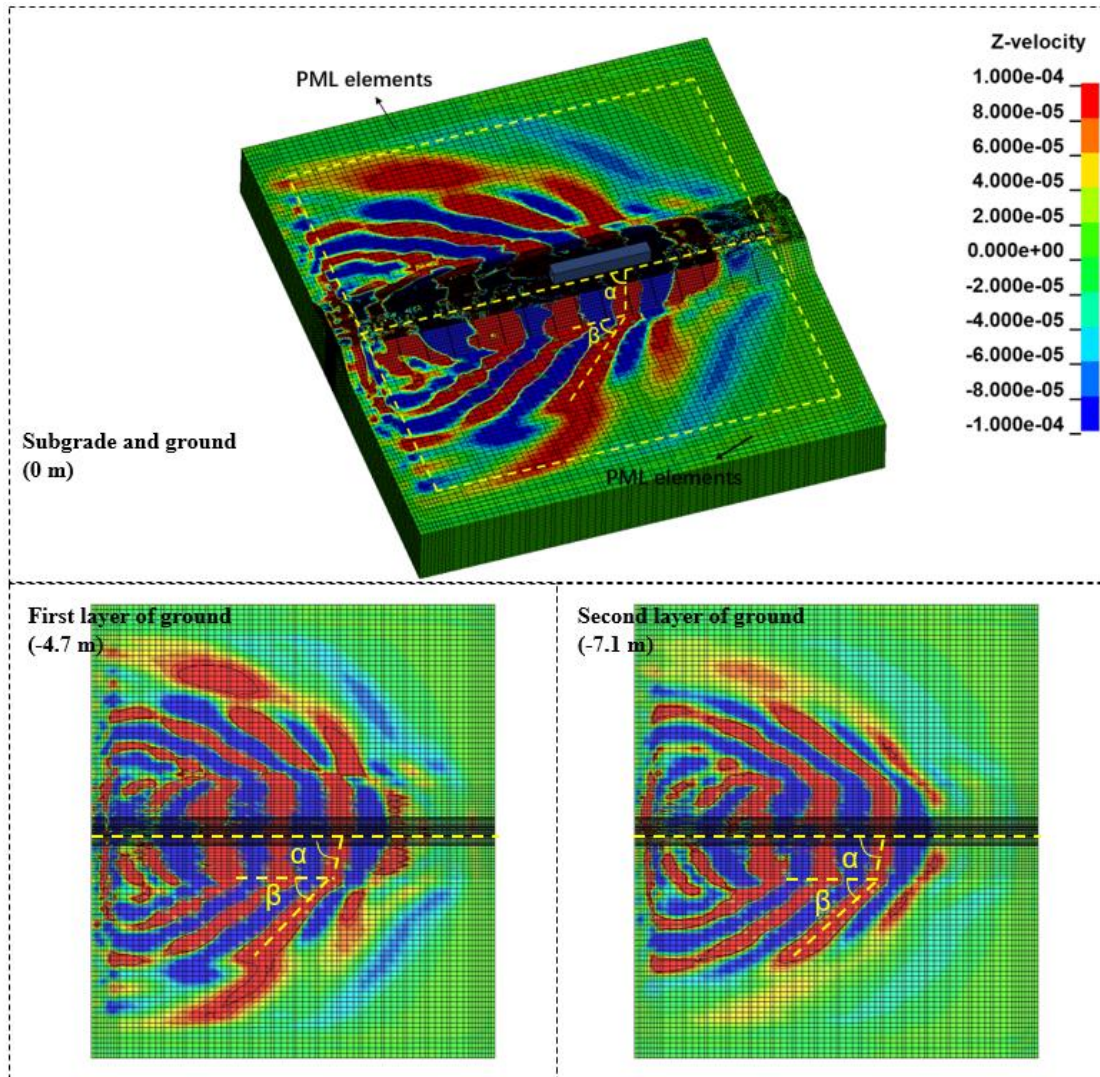
362 It is well known that three types of waves can be generated in the soils under the
363 dynamic excitation of the train-track-soil interactions: P wave, S wave, and Rayleigh wave.
364 The propagation of three types of waves is complicated in the subgrade and ground in reality.
365 In order to present an insightful and clearer wave propagation in the soils, the contours of the
366 velocity with a train speed of 440 km/h are illustrated in Figure 14. Note that the maximum
367 vertical velocity in the far-field (>50 m) is around 0.1 mm/s, the velocity was set to be
368 changed from -0.1 mm/s to 0.1 mm/s to present the wave propagations in the soils including
369 far-field. Several novel and interesting phenomena can be derived from Figure 14.



370

371

(a) Natural ground



(b) Pile-reinforced ground

Figure 14 Contours of the velocity of soils

372

373

374

375 5.1 Wavelength

376 In the natural ground case, the three upward waves (with red color) can be observed
 377 from Figure 14 (a). However, in the pile-reinforced ground case, at least four upward waves
 378 (with red color) can be observed at the same moment. The downward waves (with blue color)
 379 exhibit the same phenomenon. Therefore, the piles can interfere with the propagation of
 380 waves and accordingly decrease the wavelength of propagation waves. To the author's
 381 knowledge, this phenomenon has never been emphasized in other researches.

382 **5.2 Mach angles and propagation velocities**

383 The propagation waves angles or the so-called Mach angles (α and β) in the subgrade
 384 area and ground area are measured from the top view of the figures, and the results are shown
 385 in Table 4. Note that these angles are not the same along the longitudinal direction of the
 386 railway since every wave is trying to form a circular shape after the train passes by [9],
 387 therefore one location is chosen as an example to illustrate the differences.

388 Table 4 Mach angles

| Depth (m) | Natural ground | | Pile-reinforced ground | |
|-----------|----------------|-------------|------------------------|-------------|
| | α (°) | β (°) | α (°) | β (°) |
| 0 | 57 | - | 78 | - |
| -4.7 | 66 | 41 | 81 | 46 |
| -7.1 | 66 | 43 | 81 | 43 |

389 The Mach angles do not remain the same with the depth of soils, as shown in Table 4. In
 390 the subgrade area, the angles (α) increase with depth from subgrade (0 m) to ground (-4.7 m
 391 and -7.1m), but the angles in the ground area (β) have no apparent difference between the two
 392 layers.

393 The Mach angle can be calculated as follows [9]:

$$394 \quad \varphi_M = \arcsin \frac{1}{M_R} = \arcsin \frac{c_i}{v_0} \quad (v_0 \geq c_i, i = P, S, \text{ or } R) \quad (5)$$

395 Where M_R is the Mach number; c_i is the surface or body waves velocity in the soils; and v_0 is
 396 the train speed.

397 In the subgrade area, the dominant wave at 0 m is Rayleigh wave, but the body waves are
 398 getting decisive with depth. Since the velocities of body waves are higher than those of
 399 Rayleigh wave, the angles (α) at -4.7 m and -7.1m are higher than those at 0 m.

400 In the ground area, the difference of angles between two layers is relatively small. The
 401 propagation wave velocities can be re-calculated based on the measured Mach angles, as
 402 shown in Table 5. These propagation velocities are close to the Rayleigh wave velocity of the
 403 first layer of ground (307.43 km/h), so it is likely that the propagation waves are Rayleigh
 404 waves. Note that this method is not applicable to the subgrade waves since the train speed is

405 lower than the surface or body waves velocities of subgrade.

406 Table 5 Propagation velocities in ground

| Depth (m) | Natural ground (km/h) | Pile-reinforced ground (km/h) |
|-----------|-----------------------|-------------------------------|
| -4.7 | 288.7 | 316.5 |
| -7.1 | 300.1 | 300.1 |

407 In addition, it is noticeable that the piles can globally increase the Mach angles. Since the
408 piles can increase the stiffness of soils, the c_i in Eq.(6) will be increased, thus the Mach angles
409 are increased as well.

410 6. Conclusions

411 Most previous studies have considered only the natural ground vibration induced by
412 dynamic train loads and have completely ignored the piles effects, even though the
413 pile-reinforced ground improvement is widely adopted in high-speed railway with soft soils.
414 In order to highlight the influences of piles on the ground vibration responses, a 3D fully
415 coupled train-track-soil model has been developed based on the MBS principle, FEM theory,
416 and PML method using LS-DYNA. This is thus the world's first to investigate the pile's
417 influences on vibration responses of high-speed railway with slab tracks by a novel coupled
418 train-track-soil model with the efficient infinite boundary of PML. Based on the dynamic
419 responses from the models with natural and pile-reinforced grounds, the following novel
420 insights can be drawn:

421 (a) High-speed railway with slab tracks exhibits a considerably high critical speed. The
422 natural ground case has a critical speed of 440 km/h, while the pile-reinforced ground case
423 possesses a critical speed of 580 km/h.

424 (b) With the improvement of piles in the ground, the dynamic responses of soils such as
425 displacements, velocities, and stresses significantly decrease under the dynamic train loads.

426 (c) The train-track dynamic interaction responses are rarely influenced by the ground
427 conditions with or without piles in the high-speed railway with slab tracks.

428 (d) Piles can interfere with the propagation of waves in the soils, and thus decrease the
429 wavelength and increase the Mach angles of propagation waves.

430 **Acknowledgments**

431 This research was supported by the Key Research Development Program of China
432 (No.2016YFC0802203-2, No.2016YFC0802203-3). The authors would like to acknowledge
433 the China Scholarship Council for the financial support. The authors sincerely thank
434 European Commission for H2020-MSCA-RISE Project No. 691135 “RISEN: Rail
435 Infrastructure Systems Engineering Network,” which enables a global research network that
436 tackles the grand challenge in railway infrastructure resilience and advanced sensing under
437 extreme conditions (www.risen2rail.eu).

438 **References**

- 439 [1] Remennikov AM, Kaewunruen S. A review of loading conditions for railway track structures due to
440 train and track vertical interaction. *Structural Control Health Monitoring: The Official Journal of the*
441 *International Association for Structural Control and Monitoring and of the European Association for*
442 *the Control of Structure*. 2008;15(2):207-34.
- 443 [2] Connolly DP, Marecki GP, Kouroussis G, Thalassinakis I, Woodward PK. The growth of railway
444 ground vibration problems—a review. *Science of the Total Environment*. 2016;568:1276-82.
- 445 [3] Zhai W, Han Z, Chen Z, Ling L, Zhu S. Train–track–bridge dynamic interaction: a state-of-the-art
446 review. *Vehicle System Dynamics*. 2019;57(7):984-1027.
- 447 [4] Costa PA, Colaço A, Calçada R, Cardoso AS. Critical speed of railway tracks. Detailed and
448 simplified approaches. *Transportation Geotechnics*. 2015;2:30-46.
- 449 [5] Li T, Su Q, Shao K, Liu J. Numerical Analysis of Vibration Responses in High-Speed Railways
450 considering Mud Pumping Defect. *Shock and Vibration*. 2019;2019.
- 451 [6] Liu K, Su Q, Yue F, Liu B, Qiu R, Liu T. Effects of suffosion-induced contact variation on dynamic
452 responses of saturated roadbed considering hydro-mechanical coupling under high-speed train loading.
453 *Computers and Geotechnics*. 2019;113:103095.
- 454 [7] Feng S-J, Zhang X-L, Wang L, Zheng Q-T, Du F-L, Wang Z-L. In situ experimental study on high
455 speed train induced ground vibrations with the ballast-less track. *Soil Dynamics and Earthquake*
456 *Engineering*. 2017;102:195-214.
- 457 [8] Connolly DP, Kouroussis G, Laghrouche O, Ho C, Forde M. Benchmarking railway vibrations–
458 Track, vehicle, ground and building effects. *Construction and Building Materials*. 2015;92:64-81.
- 459 [9] Kouroussis G, Connolly DP, Verlinden O. Railway-induced ground vibrations—a review of vehicle
460 effects. *International Journal of Rail Transportation*. 2014;2(2):69-110.
- 461 [10] Thompson DJ, Kouroussis G, Ntotsios E. Modelling, simulation and evaluation of ground
462 vibration caused by rail vehicles. *Vehicle System Dynamics*. 2019;57(7):936-83.
- 463 [11] Huang H, Chrismar S. Discrete element modeling of ballast settlement under trains moving at
464 “Critical Speeds”. *Construction and Building Materials*. 2013;38:994-1000.
- 465 [12] Sheng X, Jones C, Thompson D. A theoretical study on the influence of the track on train-induced
466 ground vibration. *Journal of Sound and Vibration*. 2004;272(3-5):909-36.

467 [13] Hall L. Simulations and analyses of train-induced ground vibrations in finite element models. *Soil*
468 *Dynamics and Earthquake Engineering*. 2003;23(5):403-13.

469 [14] Dong K, Connolly DP, Laghrouche O, Woodward P, Costa PA. Non-linear soil behaviour on high
470 speed rail lines. *Computers and Geotechnics*. 2019;112:302-18.

471 [15] Shih J-Y, Thompson DJ, Zervos A. The influence of soil nonlinear properties on the track/ground
472 vibration induced by trains running on soft ground. *Transportation Geotechnics*. 2017;11:1-16.

473 [16] Kouroussis G, Verlinden O, Conti C. Influence of some vehicle and track parameters on the
474 environmental vibrations induced by railway traffic. *Vehicle System Dynamics*. 2012;50(4):619-39.

475 [17] Kouroussis G, Conti C, Verlinden O. Investigating the influence of soil properties on railway
476 traffic vibration using a numerical model. *Vehicle System Dynamics*. 2013;51(3):421-42.

477 [18] Olivier B, Connolly DP, Alves Costa P, Kouroussis G. The effect of embankment on high speed
478 rail ground vibrations. *International Journal of Rail Transportation*. 2016;4(4):229-46.

479 [19] Zhai W, Wei K, Song X, Shao M. Experimental investigation into ground vibrations induced by
480 very high speed trains on a non-ballasted track. *Soil Dynamics and Earthquake Engineering*.
481 2015;72:24-36.

482 [20] Zheng G, Jiang Y, Han J, Liu Y-F. Performance of cement-fly ash-gravel pile-supported
483 high-speed railway embankments over soft marine clay. *Marine Georesources and Geotechnology*.
484 2011;29(2):145-61.

485 [21] Lai J, Liu H, Qiu J, Chen J. Settlement analysis of saturated tailings dam treated by CFG pile
486 composite foundation. *Advances in Materials Science Engineering*. 2016;2016.

487 [22] You S, Cheng X, Guo H, Yao Z. Experimental study on structural response of CFG energy piles.
488 *Applied Thermal Engineering*. 2016;96:640-51.

489 [23] Chen Q-n, Zhao M-h, Zhou G-h, Zhang Z-h. Bearing capacity and mechanical behavior of CFG
490 pile composite foundation. *Journal of Central South University of Technology*. 2008;15(2):45-9.

491 [24] Kaewunruen S, Wang Y, Ngamkhanong C. Derailment-resistant performance of modular
492 composite rail track slabs. *Engineering Structures*. 2018;160:1-11.

493 [25] Kaewunruen S, Remennikov AM. Current state of practice in railway track vibration isolation: an
494 Australian overview. *Australian Journal of Civil Engineering*. 2016;14(1):63-71.

495 [26] Kaewunruen S, Kimani SK. Damped frequencies of precast modular steel-concrete composite
496 railway track slabs. *Steel and Composite Structures*. 2017;25(4):427-42.

497 [27] Thach P-N, Liu H-L, Kong G-Q. Vibration analysis of pile-supported embankments under
498 high-speed train passage. *Soil Dynamics and Earthquake Engineering*. 2013;55:92-9.

499 [28] Tang Y, Xiao S, Yang Q. Numerical study of dynamic stress developed in the high speed rail
500 foundation under train loads. *Soil Dynamics and Earthquake Engineering*. 2019;123:36-47.

501 [29] Connolly D, Giannopoulos A, Forde M. Numerical modelling of ground borne vibrations from
502 high speed rail lines on embankments. *Soil Dynamics and Earthquake Engineering*. 2013;46:13-9.

503 [30] Connolly D, Kouroussis G, Giannopoulos A, Verlinden O, Woodward P, Forde M. Assessment of
504 railway vibrations using an efficient scoping model. *Soil Dynamics and Earthquake Engineering*.
505 2014;58:37-47.

506 [31] Wang M, Cai C, Zhu S, Zhai W. Experimental study on dynamic performance of typical
507 nonballasted track systems using a full-scale test rig. *Proceedings of the Institution of Mechanical*
508 *Engineers, Part F: Journal of Rail and Rapid Transit*. 2017;231(4):470-81.

509 [32] Lei X, Wang J. Dynamic analysis of the train and slab track coupling system with finite elements
510 in a moving frame of reference. *Journal of Vibration and Control*. 2014;20(9):1301-17.

- 511 [33] Li T, Su Q, Kaewunruen S. Saturated Ground Vibration Analysis Based on a Three-Dimensional
512 Coupled Train-Track-Soil Interaction Model. *Applied Sciences*. 2019;9(23):4991.
- 513 [34] Li T, Kaewunruen S, Su Q, Goto K. Effects of static and dynamic material properties on vibration
514 responses of slab tracks in high speed railways. *ACOUSTICS 2019*. Milton Keynes, United Kingdom:
515 Proceedings of the Institute of Acoustics, 2019. p. 246-54.
- 516 [35] Basu U. Explicit finite element perfectly matched layer for transient three- dimensional elastic
517 waves. *International Journal for Numerical Methods in Engineering*. 2009;77(2):151-76.
- 518 [36] Wang J, Jin X, Cao Y. High-speed maglev train-guideway–tunnel–soil modelling of ground
519 vibration. *Proceedings of the Institution of Mechanical Engineers, Part F: Journal of Rail and Rapid*
520 *Transit*. 2012;226(3):331-44.
- 521 [37] You R, Goto K, Ngamkhanong C, Kaewunruen S. Nonlinear finite element analysis for structural
522 capacity of railway prestressed concrete sleepers with rail seat abrasion. *Engineering Failure Analysis*.
523 2019;95:47-65.
- 524 [38] Lee C, Bolton M, Al-Tabbaa A. Numerical modelling of group effects on the distribution of
525 dragloads in pile foundations. *Geotechnique*. 2002;52(5):325-35.
- 526 [39] Shengcai Y. Calculation and Assessment Analysis of the Dynamic Performance for Slab Track on
527 Sui-Yu Railway. Chengdu: Southwest Jiaotong University, 2007.
- 528 [40] Cai C, Zhai W, Wang K. Calculation and Assessment Analysis of the Dynamic Performance for
529 Slab Track on Sui-Yu Railway. *China Railway Science*. 2006;04:17-21.
- 530 [41] Hu J, Bian X, Xu W, Thompson D. Investigation into the critical speed of ballastless track.
531 *Transportation Geotechnics*. 2019;18:142-8.
532